Top Catal (2017) 60:782–788
DOI 10.1007/s11244-017-0770-8

ORIGINAL PAPER

The Effect of Solvent on the Synthesis of $BiVO_4$ Using Solvothermal Method and Their Photocatalytic Activity Under Visible Light Irradiation

Duy Trinh Nguyen[1] · Seong-Soo Hong[1]

Published online: 10 April 2017

Abstract A monoclinic-tetragonal heterostructure of $BiVO_4$ was successfully synthesized by performing a solvothermal method using different molar ratio of EGME/H_2O as mixed solvents. The phase structure and morphology of as-prepared $BiVO_4$ samples were characterized by Raman spectroscopy, XRD, SEM and DRS. We have also investigated the photocatalytic activity of these materials for the decomposition of Rhodamine B under visible light irradiation. When $BiVO_4$ was synthesized using a mixture of EGME and H_2O solvents (EGME/H_2O volume ratio varied from 70/10 to 10/70), XRD pattern showed the coexistence of monoclinic and tetragonal phase. From the XRD, Raman spectroscopy and SEM results, the monoclinic-tetragonal heterostructure of $BiVO_4$ samples prepared using different volume ratios of EGME/H_2O exhibited different morphologies and crystal structure. The $BiVO_4$ catalyst, which was prepared when the volume ratio of EGME/water was set at 40/40, showed the highest photocatalytic activity in the photodegradation of Rhodamine B under visible light.

Keywords Monoclinic-tetragonal heterostructured $BiVO_4$ · Solvothermal method · EGME/water mixed solvent · Photodecomposition of Rhodamine B

1 Introduction

Bismuth(III) vanadate ($BiVO_4$), a member of the Aurivillius family of layered oxides, has been extensively used in photocatalytic applications. It exhibits high photooxidative capacity as a catalyst during the evolution of O_2 from water [1, 2]. It is also used as a catalyst in the reduction of carbon dioxide [3] and in the decomposition of organic pollutants under the effect of sunlight [4, 5]. It is a well-known fact that $BiVO_4$ has three types of crystal structures: monoclinic scheelite (s-m), tetragonal zircon (z-t), and tetragonal scheelite (s-t) structures [6]. Different preparation routes are used to selectively synthesize these crystalline structures. Among the aforementioned structures, s-m $BiVO_4$ exhibits the highest photocatalytic activity in the presence of visible light; this photocatalytic activity can be attributed to the electronic structure and optical properties of s-m $BiVO_4$. It has a narrow band gap (2.4 eV), because when it absorbs visible light, the an electron is excited from a valence band or a hybrid orbital of Bi 6s and O 2p to a conduction band of V 3d [7]. However, owing to poor charge transport characteristics and weak surface adsorption, there is recombination of excessive electrons and holes. As a result, the photocatalytic activity of s-m $BiVO_4$ is restricted.

Many researchers have various strategies to improve photocatalytic performance by facilitating the separation of electron–hole pairs. For example, three approaches have been recently applied on $BiVO_4$: (I) the formation of a p-n junction and the establishment of an internal electric field that extends from the n-type ($BiVO_4$) to p-type semiconductor [8, 9], (II) a control over the morphology and crystallographic facets; (III) the formation of a monoclinic-tetragonal heterostructure of $BiVO_4$ [10, 11]. Notably, a monoclinic-tetragonal heterostructure of $BiVO_4$ can indeed improve the photocatalytic activity. Tan et al. have reported that compared to m-s $BiVO_4$ and t-z $BiVO_4$, a monoclinic-tetragonal heterostructure of $BiVO_4$ can be produced by adjusting the pH of precursors, showing higher

✉ Seong-Soo Hong
sshong@pknu.ac.kr

[1] Department of Chemical Engineering, Pukyong National University, 365 Shinseonro, Busan 48547, South Korea

photocatalytic efficiency under UV and simulated sunlight [12]. On the other hand, Usai et al. synthesized a monoclinic-tetragonal heterostructure of $BiVO_4$ by yttrium doping [13]. They also reported about higher photocatalytic activity, which was achieved at an interface of monoclinic-tetragonal heterophase, which dominated the spatial condition of charge transfer by favoring the separation of photoinduced electron–hole pairs and changing the migration direction of photoinduced carriers. Hu and coworkers also adopted a similar strategy and conducted electrochemical measurement using electron paramagnetic resonance (EPR) and photoluminescence (PL) techniques [14]. Nevertheless, it is still quite challenging to ensure a facile and reproducible synthesis of $BiVO_4$, having a monoclinic-tetragonal heterostructure. Our previous study showed that we have developed a facile formation of the monoclinic-tetragonal heterostructure of $BiVO_4$ using EGME-H_2O as mixed solvents [15].

In this study, we have prepared a tetragonal-monoclinic heterostructure of $BiVO_4$ by solvothermal method using different molar ratio of EGME-H_2O as mixed solvents. The physical properties of as-prepared $BiVO_4$ samples were characterized by Raman spectroscopy, X-ray diffraction pattern (XRD), scanning electron microscopy (SEM), and diffuse reflectance UV–Visible spectroscopy (UV–Vis DRS). We have also investigated whether the photocatalytic activity of these materials can bring about the decomposition of Rhodamine B in the presence of visible light.

2 Experimental

Since all the chemicals were of analytical grade, no further purification was performed. We prepared various morphologies of $BiVO_4$ photocatalysts using a solvothermal method. In this method, we mixed the solvent of ethylene glycol monomethyl ether (EGME) with water in different volume ratio. Briefly, $Bi(NO_3)_3$ (4 mmol, 1.98 g) and Na_3VO_4 (4 mmol, 0.74 g) were dissolved in 0–80 mL of EGME and 80–0 mL of H_2O, respectively. These two solutions were mixed together and stirred for 1 h to prepare a homogeneous solution that was orange in color. The mixture was transferred into a Teflon-coated stainless steel bomb and heated at 100 °C for 12 h. After each reaction, the resultant suspension was centrifuged at 10,000 rpm for 10 min. As a result, the $BiVO_4$ solids got accumulated at the bottom of the tube and then this tube was rinsed with water and ethanol several times. Thereafter, it was dried overnight at 60 °C. Finally, it was calcined at 300 °C for 3 h.

The crystal structures of $BiVO_4$ samples were examined from the powder X-ray diffraction (XRD) patterns, which were obtained using Cu Kα radiation (λ = 1.5405 Å) in the 2θ range of 5–30°; a scan rate of 1.0 °/min was maintained (Rigaku Co., Model DMax). Raman spectra were recorded by operating a micro Raman spectrometer (Dongwoo Optron, MonoRa500i) in a wavelength range of 200 to 1000 cm^{-1}; a laser beam of 785 nm. The morphology of the products was observed under a scanning electron microscope (SEM, JEOL JSM6700F), which was operated at an accelerating voltage of 3 kV. The UV–Visible diffuse reflectance spectrum (UV–Vis DRS) of the products was recorded on a Varian Cary 100 using polytetrafluoroethylene (PTFE) as the standard.

We calculated the photocatalytic activities of samples after performing photocatalytic decomposition of RhB under visible light using a 300 W Xe-arc lamp (Oriel) and a 410 nm cut-off filter. The light was passed through a 10 cm thick IR water filter, and then it was focused onto a 150 mL Pyrex using a quartz window. The pH value of the solution was maintained at 7.0; the temperature of the solution was maintained within a range of 23–25 °C. To determine the catalytic activity in these experiments, the reactor was filled with a mixture of RhB aqueous solution (10^{-5} M, 100 mL) and the given photocatalyst (100 mg). Before irradiation, the mixture was magnetically stirred in dark conditions for 60 min. Thus, we ensured an adsorption–desorption equilibrium between the surface of the photocatalyst and the organic molecules. At regular time intervals, we withdrew 3 mL of the suspension and filtered it through a 0.22 μm membrane filter to produce a clear solution. A decrease in the concentration of RhB solution was determined with a UV–Visible spectrophotometer (Mecasys Optizen Pop) at λ = 554 nm.

3 Result and Discussion

Figure 1 shows the XRD patterns of the as-synthesized $BiVO_4$ samples, which were prepared using different volume ratios of EGME/H_2O. When only EGME (EGME/H_2O = 80/0) was used as the solvent, the XRD pattern of the product exhibited a pattern that was similar to that of s-m $BiVO_4$. When $BiVO_4$ was synthesized using a mixture of EGME and H_2O solvents (EGME/H_2O volume ratio varied from 70/10 to 10/70), XRD pattern depicted the coexistence of monoclinic and tetragonal phase. Since V_{EGME} decreased with an increase of V_{water}, the relative intensity of the peak (121) of the monoclinic phase decreased, while the relative intensity of the peak (200) of the tetragonal phase increased.

When we used a mixture of EGME and water as the solvent, the XRD pattern revealed a mixture of monoclinic and tetragonal phases; the (121) peak was attributed to the monoclinic phase (2θ = 29°), while the (200) peak was attributed to the tetragonal phase (2θ = 24.4°). We obtained the normalized ratio of relative intensities of (121) peak

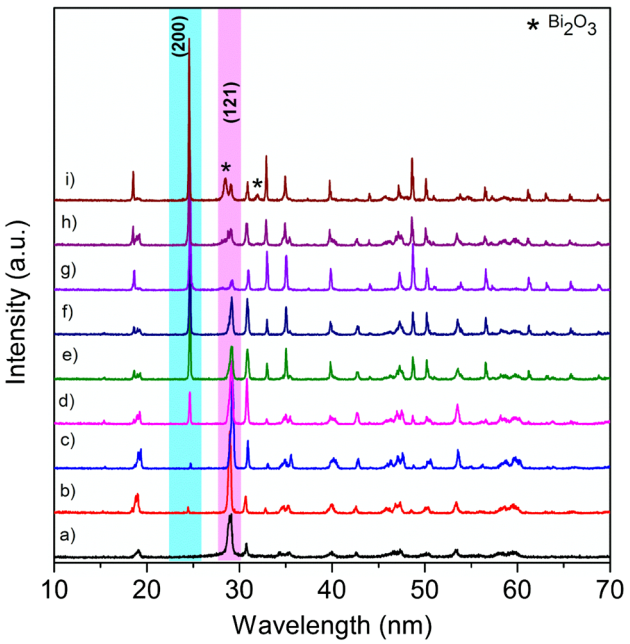

Fig. 1 XRD patterns of $BiVO_4$ samples prepared using different volume ratios of EGME/H_2O: (*a*) 80/0, (*b*) 70/10, (*c*) 60/20, (*d*) 50/30, (*e*) 40/40, (*f*) 30/50, (*g*) 20/60, (*h*) 10/70 and (*i*) 0/80

Table 1 The physical properties and photocatalytic activity of $BiVO_4$ catalysts prepared using different volume ratios of EGME/H_2O

Sample	Solvent	$V_{solvent}/V_{water}$ (ml/mL)	η_{mono} (%)	E_{bg} (eV)	k ($\times 10^{-3}$ min^{-1})
1	EGME	80/0	100	2.35	4.0
2	EGME	70/10	95.50	2.29	4.4
3	EGME	60/20	93.65	2.38	26.4
4	EGME	50/30	66.25	2.42	20.0
5	EGME	40/40	22.14	2.43	40.5
6	EGME	30/50	22.23	2.42	20.4
7	EGME	20/60	7.20	2.42	15.4
8	EGME	10/70	7.11	2.45	17.9
9	EGME	0/80	4.29	2.40	7.6

that represents the monoclinic phase [$I_{mono(121)}$] and (200) peak that represents tetragonal phase [$I_{tetra(200)}$]. Then, we estimated the percentage of monoclinic phase (η_{mono}) in the hererostructure of $BiVO_4$ samples:

$$\eta_{mono} = \frac{I_{mono(121)}}{I_{mono(121)} + I_{tetra(200)}} \times 100$$

The obtained η_{mono} values are shown in Table 1. As shown in Table 1, m-$BiVO_4$ percentage decreases from 100 to 7.22% when V_{water} is increased from 0 to 70 mL. This result indicates that the tetragonal-monoclinic heterostructure of $BiVO_4$ can be simply synthesized by controlling the EGME/H_2O volume ratio. The presence of EGME can promote the formation of m-$BiVO_4$, while the addition of H_2O can promote the formation of t-$BiVO_4$. However, when only H_2O (EGME/H_2O = 0/80) was used as the solvent, the XRD pattern of the product was similar to that of z-t $BiVO_4$; however, the XRD pattern also depicted the coexistence of Bi_2O_3, which is formed from the hydrolysis of $Bi(NO_3)_3$.

Figure 2 shows the Raman spectra of $BiVO_4$ samples prepared at different volume ratios of EGME/H_2O. According to previous reports, Raman spectra of $BiVO_4$ samples can be excited by a green (532 nm) and a red (785 nm) laser. However, we could clearly observe all Raman bands of $BiVO_4$, which were excited by a green laser. This is because the penetration depth of a red laser into a crystal differs from that of a green laser [16, 17]. Therefore, all the samples were excited at 785 nm. We found that the monoclinic phase of $BiVO_4$ sample has six Raman-active modes: the external mode of $BiVO_4$ (210 cm^{-1}), the asymmetric deformation mode of VO_4^{3-} (324 cm^{-1}), the symmetric deformation mode of VO_4^{3-} (366 cm^{-1}), the asymmetric stretching mode of V–O bonds (640 and 710 cm^{-1}), and the symmetric stretching mode of V–O bonds (820 cm^{-1}) [16]. The Raman spectrum of tetragonal zircon phase of $BiVO_4$ sample is characterized by four modes: the Bi–O stretching mode (255 cm^{-1}), the V–O–V bending mode (373 cm^{-1}), the antisymmetric V–O stretching mode (764 cm^{-1}), and the symmetric V–O stretching mode (858 cm^{-1}) [18]. As shown in Fig. 2, the Raman spectrum illustrates the transition of monoclinic to tetragonal phase in $BiVO_4$ samples, which were synthesized using different volume ratios of EGME/H_2O. In the Raman spectra, we observe the transition of the ν_s(V–O) band shift from 810 to 860 cm^{-1}. Owing to the transition, we also observe the disappearance of the $\delta(VO_4^{3-})$ doublet of the monoclinic phase, the appearance of the antisymmetric V–O stretching mode (764 cm^{-1}) of the tetragonal phase, and the appearance of the Bi–O stretching mode (255 cm^{-1}) of the tetragonal phase. This result provides further evidence that $BiVO_4$ exhibits a tetragonal-monoclinic heterostructure, which can be simply synthesized by controlling the volume ratio of EGME/H_2O.

Figure 3 shows SEM images of $BiVO_4$ samples, which were prepared using different volume ratios of EGME/H_2O. It is clearly seen that the volume ratio of EGME/H_2O has an obvious influence on the morphologies of $BiVO_4$ products. When only EGME (EGME/H_2O = 80/0) was used as the solvent, the morphology of the synthesized $BiVO_4$ consisted of aggregated nanoparticles. When water was introduced in the system, the $BiVO_4$ products show different morphologies, corresponding to the increase of V_{water}. Olive-like m-s $BiVO_4$ was obtained when the volume ratio

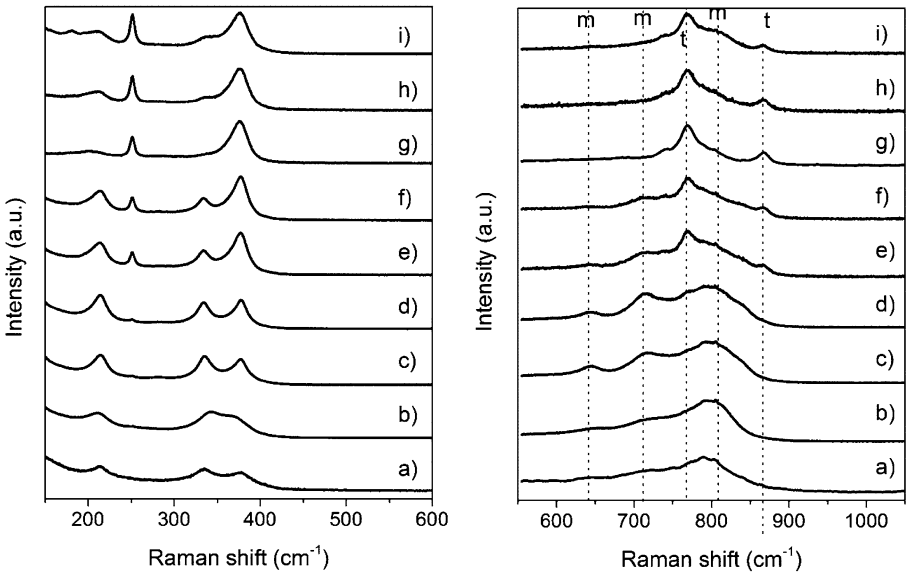

Fig. 2 Raman spectra of $BiVO_4$ samples prepared using different volume ratios of EGME/H_2O: (*a*) 80/0, (*b*) 70/10, (*c*) 60/20, (*d*) 50/30, (*e*) 40/40, (*f*) 30/50, (*g*) 20/60, (*h*) 10/70 and (*i*) 0/80

of EGME/water was set at 70/10. After adjusting the volume ratio of EGME/water to 60/20, the sample exhibited an amorphous morphology as it contained a large number of particles that were irregular in size. When the volume ratio of EGME/water was changed to 50/30, some rod-like particles began to appear along with a large amount of irregular particles. Similarly, rod-like morphology was obtained when the volume ratio of EGME/water was changed to 40/40, 50/30, 60/20, and 70/10. However, as the volume of water (V_{water}) was increased in the medium, the length of these rods seemed to increase while the width of these rods began diminishing. The final $BiVO_4$ product, which exhibited a rod-like morphology, was also obtained when only H_2O (EGME/H_2O = 0/80) was used as the solvent. From the XRD, Raman, and SEM results, we conclude that monoclinic-tetragonal heterostructure of $BiVO_4$ samples prepared using different volume ratios of EGME/H_2O exhibit different morphologies under different solvothermal conditions.

The light absorption properties of photocatalysts were examined in DRS. Figure 4 shows the DRS spectra of as-prepared $BiVO_4$ samples. As shown in Fig. 4, all the catalysts displayed strong absorption in the visible range of the electromagnetic spectrum. Owing to the absorbance of visible light, the photocatalytic property of $BiVO_4$ materials was enhanced in the visible region of electromagnetic spectrum. The indirect band gap energy (E_g) of all the samples was calculated from the tangent lines obtained in the plots of modified Kubelka–Munk function $[F(R'_\infty)h\vartheta]^{1/2}$ versus photon energy. The band gap values of various $BiVO_4$ samples are presented in Table 1. As shown in Table 1, the band gap values of $BiVO_4$ catalysts prepared using different volume ratios of EGME/H_2O are shown to have similar value from 2.29 to 2.45 eV.

In order to evaluate the photocatalytic activities of the $BiVO_4$ samples prepared using different volume ratios of EGME/H_2O, we investigated the degradation ability of Rhodamine B dye in water in the presence of visible light. Figure 5 shows the temporal evolution of the UV–Vis spectra produced by the photodegradation of Rhodamine B dye. In this reaction, monoclinic-tetragonal heterostructure of $BiVO_4$ sample was used as the photocatalyst in the presence of visible light ($\lambda > 400$ nm). As seen in the above spectra, the absorption of Rhodamine B/m-t heterostructure of $BiVO_4$ and suspensions gradually decreased during the photodegradation process. In addition, the major absorption peak, which corresponds to RhB, was shifted from 554 to 500 nm in a step-wise manner. Thus, the ethyl groups were removed one by one in this reaction. This finding is in good agreement with the previous literature [16].

It is a well-known fact that the photocatalytic oxidation of organic pollutants follows Langmuir–Hinshelwood kinetics [19], where the rate is proportional to the coverage θ:

$$r = -\frac{dC}{dt} = k\theta = k\frac{KC}{1+KC} \quad (1)$$

here, k is the true rate constant; it is dependent upon various parameters, such as the mass of the catalyst, the flux efficiency, and oxygen coverage. K is the adsorption coefficient of the reactant, and C is the concentration of the reactant. When C is very small, the product KC is negligible with respect to unity. Under these conditions, Eq. (1) represents a first-order kinetic reaction. When the parameters of Eq. (1) are set to the initial conditions of a photocatalytic procedure, $t = 0$ and the concentration can be given as $C = C_0$. Substituting these initial values of reactions in Eq. (1), we obtain Eq. (2) as follows

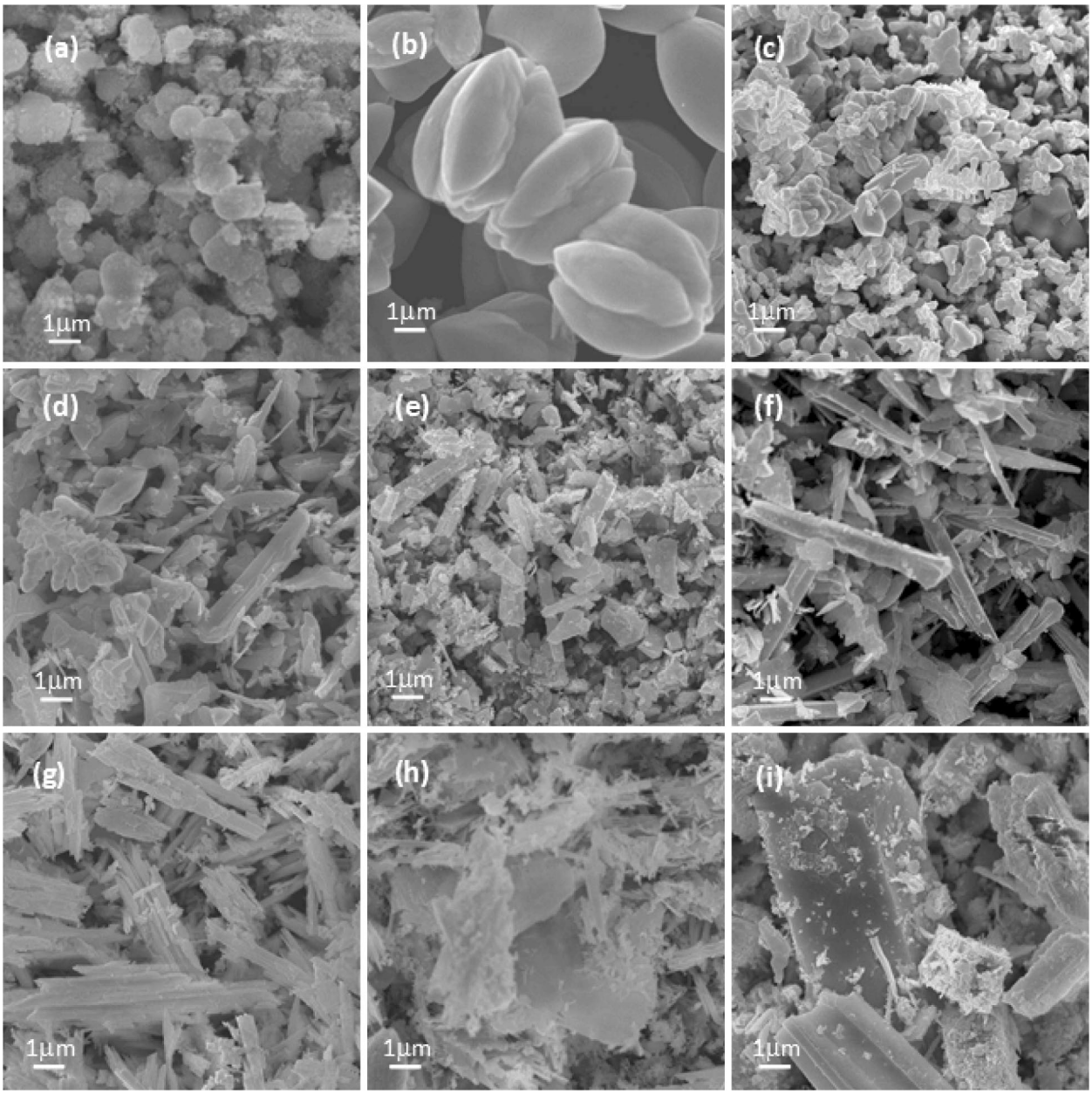

Fig. 3 SEM images of $BiVO_4$ samples prepared using different volume ratios of EGME/H_2O: **a** 80/0, **b** 70/10, **c** 60/20, **d** 50/30, **e** 40/40, **f** 30/50, **g** 20/60, **h** 10/70 and **i** 0/80

$$-\ln\left(C/C_o\right) = k_{app}t \quad (2)$$

where k_{app} is the apparent first-order reaction constant.

In Fig. 6 and Table 1, we have presented how visible light influences the photocatalytic activity associated with the decomposition of Rhodamine B over $BiVO_4$ samples, which were prepared using different volume ratios of EGME/H_2O. When a blank test was carried out in the absence of the photocatalyst, about 7% of the Rhodamine B was decomposed after 2 h by the photolysis reaction. As shown in Table 1, the $BiVO_4$ catalyst, which was prepared when the volume ratio of EGME/water was set at 40/40, showed the highest photocatalytic activity in the photodegradation of Rhodamine B under visible light. The k_{app} value of tetragonal-monoclinic heterophase of $BiVO_4$ catalyst was 40.5×10^{-3} min^{-1}.

The enhanced photocatalytic activity of $BiVO_4$ samples is most probably related to the surface-phase junctions, which are formed between monoclinic scheelite and tetragonal zircon. In pure s-m $BiVO_4$ catalyst, the pathway of photocatalytic degradation includes the

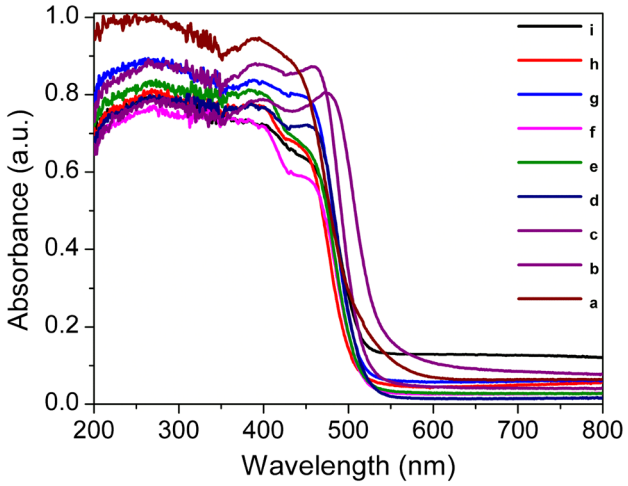

Fig. 4 UV–Vis diffuse reflectance spectra of $BiVO_4$ samples prepared using different volume ratios of EGME/H_2O: (*a*) 80/0, (*b*) 70/10, (*c*) 60/20, (*d*) 50/30, (*e*) 40/40, (*f*) 30/50, (*g*) 20/60, (*h*) 10/70 and (*i*) 0/80

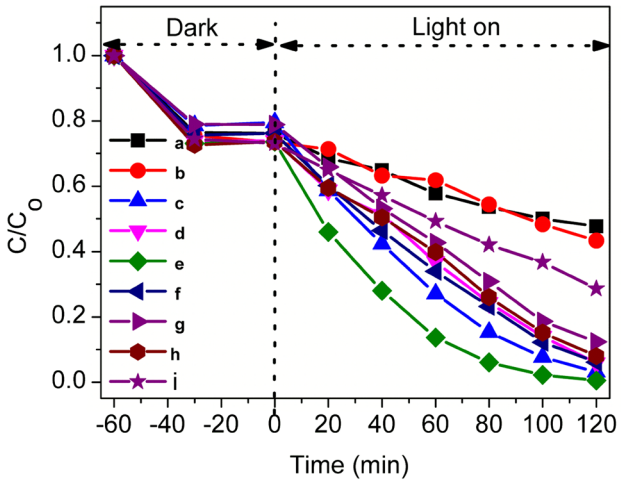

Fig. 6 Photocatalytic decomposition of Rhodamine B over $BiVO_4$ samples prepared using different volume ratios of EGME/H_2O: (*a*) 80/0, (*b*) 70/10, (*c*) 60/20, (*d*) 50/30, (*e*) 40/40, (*f*) 30/50, (*g*) 20/60, (*h*) 10/70 and (*i*) 0/80

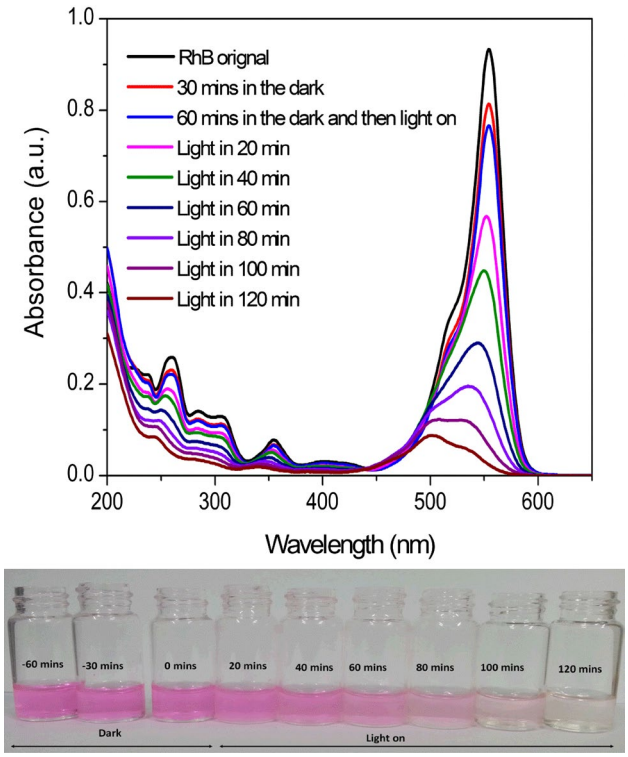

Fig. 5 UV–Vis absorption spectra of RhB solution separated from catalyst suspensions during illumination using $BiVO_4$ sample prepared using volume ratios of EGME/H_2O(40/40)

following steps: (1) the formation of photogenerated hole (h^+) and electron (e^-) occurs due to the absorption of visible light; (2) the $h^+$and e^- diffuse into the $BiVO_4$ surface; (3) the h^+ react with adsorbed water molecules, forming hydroxyl radicals (·OH). Then, the h^+ and the ·OH radicals oxidize in the nearby Rhodamine B molecules, which are present on the $BiVO_4$ surface. In the second step, there is recombination of a large proportion of electron hole pairs. Consequently, the photocatalytic activity of s-m $BiVO_4$ is limited. However, we found that the particular tetragonal-monoclinic heterostructure of $BiVO_4$ sample promotes the separation of photoinduced electron–hole pairs [13]. Thus, in the tetragonal-monoclinic heterostructure of $BiVO_4$ catalyst, the tetragonal phase acts as an electron acceptor to bring about the photocatalytic decomposition of organic dyes. Thus, the recombination of electron–hole pairs is prevented. Such an enhancement in the photocatalytic activity of the heterostructure of $BiVO_4$ sample is achieved by optimizing the separation of electron–hole pairs. In addition, it was reported that the formation process of tetragonal-monoclinic heterostructure of $BiVO_4$ samples consists of two steps: nucleation and aggregation growth process [15]. When the $BiVO_4$ nuclei aggregate in the EGME/H_2O media in the second stage, the $BiVO_4$ samples show the different morphology. It is well known that the photocatalytic activities of nanostructured catalyst strongly rely on their size and shapes due to the morphology-property relationship at the nanoscale [20]. Therefore, the $BiVO_4$ catalyst, which was prepared when the volume ratio of EGME/water was set at 40/40, showed the tetragonal-monoclinic heterostructure and rod-like shapes to have high photocatalytic activity.

4 Conclusions

We have prepared a monoclinic-tetragonal heterostructure of $BiVO_4$ by solvothermal method using different volume ratios of EGME/H_2O. Thereafter, we characterized these $BiVO_4$ samples by the following techniques: X-ray diffraction pattern (XRD), Raman spectroscopy, scanning electron microscopy (SEM) and diffuse reflectance UV–Visible spectroscopy (UV–Vis DRS). We also investigated the photocatalytic activity of these materials for the decomposition of Rhodamine B under visible light irradiation. When $BiVO_4$ was synthesized using different volume ratio of EGME/H_2O solvents, XRD pattern depicted the coexistence of monoclinic and tetragonal phase. In addition, the monoclinic-tetragonal heterostructure of $BiVO_4$ samples prepared using different volume ratios of EGME/H_2O exhibited different morphologies and crystal structure. The $BiVO_4$ catalyst, which was prepared when the volume ratio of EGME/water was set at 40/40, showed the highest photocatalytic activity in the photodegradation of Rhodamine B under visible light. This result indicates that the ratio of EGME/H_2O play an important role in controlling the morphology and the photocatalytic activity.

Acknowledgements This research was supported by Basic Science Research Program through the National Research Foundation of Korea (**NRF**) funded by the Ministry of Education, Science and Technology.

References

1. Ke D, Peng T, Ma L, Cai P, Dai K (2009) Inorg Chem 48:4685–4691
2. Tokunaga S, Kato H, Kudo A (2001) Chem Mater 13:4624–4628
3. Liu Y, Huang B, Dai Y, Zhang X, Qin X, Jiang M, Whangbo MH (2009) Catal Commun 11:210–213
4. Kohtani S, Koshiko M, Kudo A, Tokumura K, Ishigaki Y, Toriba A, Hayakawa K, Nakagaki R (2003) Appl Catal B 46:573–586
5. Guangcheng X, Jinhua Y (2010) Chem Commun 46:1893–1895
6. Lim AR, Choh SH, Jang MS (1995) J Phys Condens Matter 7:7309–7323
7. Kudo A, Omori K, Kato H (1999) J Am Chem Soc 121:11459–11467
8. Mandi H, Ting S, Yun TP, Xiaofeng C, Kiang TO, Siu TM (2013) RSC Adv 3:24964–24970
9. Weirong Z, Yan W, Yong Y, Jing T, Yanan Y (2012) Appl Catal B 115–116:90–99
10. Fan H, Jiang T, Li H, Wang D, Wang L, Zhai J, He D, Wang P, Xie T (2012) J Phys Chem C 116:2425–2430
11. Long M, Cai W, Kisch H (2008) J Phys Chem C 112:548–554
12. Tan G, Zhang L, Ren H, Wei S, Huang J, Xia A (2013) ACS Appl Mater Interfaces 5:5186–5193
13. Usai S, Obregón S, Becerro AI, Colón G (2013) J Phys Chem C 117:24479–24484
14. Hu Y, Li D, Sun F, Wang H, Weng Y, Xiong W, Shao Y (2015) RSC Adv 5:54882–54889
15. Nguyen TD, Hong SS (2017) J Nanosci Nanotechnol 17:2690–2694
16. Obregón S, Colón G (2014) Appl Catal B 158–159:242–249
17. Yu J, Kudo A (2006) Adv Funct Mater 16:2163–2169
18. Li G, Bai Y, Zhang WF (2012) Mater Chem Phys 136:930–934
19. Jung WY, Hong SS (2013) J Ind Eng Chem 19:157–160
20. Li G, Zhang D, Yu JC (2009) Chem Mater 20:3983–3986